


# Preparation of CuS/ZnS/G-C<sub>3</sub>N<sub>4</sub> Nanocomposite and its Photocatalytic Hydrogen Production Performance

ISSN : 2688-8394



**\*Corresponding author:** Haixia Liu, Shandong Provincial Key Laboratory of Molecular Engineering, School of Chemistry and Chemical Engineering, Qilu University of Technology (Shandong Academy of Sciences), Jinan 250353, China

**Submission:**  May 05, 2023

**Published:**  May 25, 2023

Volume 4 - Issue 1

**How to cite this article:** Bensheng Lin and Haixia Liu\*. Preparation of CuS/ZnS/G-C<sub>3</sub>N<sub>4</sub> Nanocomposite and its Photocatalytic Hydrogen Production Performance. Ann Chem Sci Res. 4(1). ACSR. 000579. 2023. DOI: [10.31031/ACSR.2023.04.000579](https://doi.org/10.31031/ACSR.2023.04.000579)

**Copyright@** Haixia Liu\*. This article is distributed under the terms of the Creative Commons Attribution 4.0 International License, which permits unrestricted use and redistribution provided that the original author and source are credited.

**Bensheng Lin and Haixia Liu\***

Shandong Provincial Key Laboratory of Molecular Engineering, School of Chemistry and Chemical Engineering, Qilu University of Technology (Shandong Academy of Sciences), China

## Abstract

CuS/ZnS heterojunction was formed by cation exchange of defective ZnS, and g-C<sub>3</sub>N<sub>4</sub> was loaded by ultrasonic impregnation method. A CuS/ZnS/g-C<sub>3</sub>N<sub>4</sub> nanocomposite with good visible light response was developed. The CuS/ZnS/g-C<sub>3</sub>N<sub>4</sub> nanocomposites were analyzed and tested by various characterization methods to determine the composition of the composites, and to study their morphology and performance. The hydrogen production capacity was tested by PLS series simulated solar xenon lamp light source with 0.25M NaS and 0.35M Na<sub>2</sub>SO<sub>4</sub> as sacrificial agents. The results show that the prepared CuS/ZnS/g-C<sub>3</sub>N<sub>4</sub> nanocomposites have good activity relative to the defect zinc sulfide and CuS/ZnS. The hydrogen production effect of g-C<sub>3</sub>N<sub>4</sub> containing 5wt% under visible light is 2265.87umol/g.h, which has good visible light responsiveness. The excellent performance of this material is mainly due to its enhanced visible light absorption capacity and difficult recombination of electrons and holes.

**Keywords:** Hetero junction; Photo-responsive; Nanocomposite material; Visible light

## Introduction

The increasingly serious energy crisis has become a global problem. In order to promote the sustainable development of the country and society, researchers have begun to study photocatalytic water splitting. Since Fujishima first discovered that titanium dioxide decomposes water into oxygen and hydrogen under the excitation of ultraviolet light in 1972 [1], titanium dioxide has entered peoples field of vision. Titanium dioxide has good light stability and non-toxicity [2-5]. However, titanium dioxide has a large band gap (3.2eV), which limits its full use of visible light. So, scientists began looking for new materials to replace titanium dioxide. ZnS is an n-type semiconductor with good photocatalytic hydrogen production effect. Compared with titanium dioxide, it has fast photogenerated carriers, high efficiency and long life. Although the band gap of ZnS gap (3.6-3.8 eV), its reduction potential is about 1.3 eV higher than that of titanium dioxide and it is easy to be doped with (non) metal ions [6-8], This brings infinite possibilities to ZnS materials. It has been reported that in order to expand the responsiveness of visible light, metal elements (Cu Ni Cd.....) are introduced into zinc sulfide and non-metallic elements (CN) to enhance the visible light responsiveness of zinc sulfide [9-14].

As far as we know, materials can be modified not only by doping, but also by changing the properties of the material itself to enhance its performance, such as defect state, exposed surface, crystal surface, etc [15-17]. Crystal defects are very hot in your research in recent years. The new energy levels generated can effectively reduce the band gap and inhibit the recombination of photogenerated carriers. However, it is very important to control the number of defects. If the number of defects is too large, defects can provide sites for carrier recombination, which greatly reduces the photocatalytic activity. For example, oxygen vacancy is a common crystal defect, which plays an important role in improving photocatalytic response in titanium dioxide [18-21], zinc oxide [22,23] and iron oxide [24] photocatalysts. In recent reports, the S and Zn vacancies of zinc sulfide can induce good photocatalytic performance under visible light. The activity of zinc sulfide photocatalyst can increase with the increase

of S vacancy concentration. Zn vacancies are also beneficial to increase the photo-response under visible light and reduce the band gap of zinc sulfide. Therefore, we can regulate the defects of zinc sulfide to prepare a defective zinc sulfide with good light responsiveness.  $g\text{-C}_3\text{N}_4$  is a good catalyst that has attracted much attention recently, mainly due to its high stability, easy availability and environmental friendliness. The mixture of melamine and urea [25-29] can be calcined to synthesize  $g\text{-C}_3\text{N}_4$ . It has good visible light responsiveness, and its band gap is 2.6eV, which is a very ideal hydrogen production photocatalyst. Unfortunately, the electrons and holes produced by it are easily recombined and have low stability. Therefore, people began to increase their porosity by combining with other materials [30-32] and doping metal or nonmetal. Among them, heterojunction recombination seems to be the most effective means, because heterojunction is conducive to the separation of electrons and holes.

In this study, we constructed defective zinc sulfide by hydrothermal method, then prepared CuS/ZnS by cation exchange method, and finally synthesized CuS/ ZnS/ $g\text{-C}_3\text{N}_4$  nanocomposites by ultrasonic impregnation method and stirring. The material has good photocatalytic hydrogen production performance under visible light.

## Materials and Methods

### Chemicals

Ethanolamine, melamine, thiourea,



### Sample preparation

#### Preparation of ZnS

Spherical zinc sulfide was synthesized by ethanolamine-assisted solvothermal method. 2.23g zinc nitrate hexahydrate and 0.76g thiourea were dissolved in 30ml deionized water and 10ml ethanolamine. Then 0.5g PVP was added under magnetic stirring for 1h. The resulting solution was placed in a 100ml polytetrafluoroethylene-lined reactor. The reaction was carried out at 180 °C for 4h. Finally, the reaction kettle was cooled to room temperature naturally. After several centrifugal washing, the pink precipitate was obtained and dried at 65 °C for 12h.

#### Preparation of CuS/ZnS

CuS/ZnS nanocomposites were synthesized by cation exchange method [33]. The synthesized ZnS (0.4628g) was dissolved in 40ml deionized water, ultrasonically dispersed for 30min, added with 0.0604g of copper nitrate trihydrate, and then magnetically stirred for 6h. After several centrifugation and washing, it was dried overnight at 65 °C.

#### Preparation of $g\text{-C}_3\text{N}_4$

Melamine (5g) was placed in a porcelain crucible and calcined in a temperature-programmed muffle furnace at a heating rate of 3 °C/min to 550 °C for 2h. Naturally cool to room temperature to obtain yellow flocs, which are ground to powder with a mortar.

#### Preparation of CuS/ZnS/ $g\text{-C}_3\text{N}_4$

The prepared  $g\text{-C}_3\text{N}_4$  powder was dissolved in 20ml of anhydrous ethanol and 20ml of deionized water, dispersed by ultrasonic dispersion for 30min, added with 0.285g of synthesized CuS/ZnS powder, and then stirred on a magnetic stirrer for 6h. The resulting solution was centrifuged and dried and dried in an oven at 65 °C for 12h to obtain the final product. CuS/ZnS/ $g\text{-C}_3\text{N}_4$  nanocomposites were obtained by changing the weight of  $g\text{-C}_3\text{N}_4$  by 5,10,15wt%, and the final product was named CZ-5%, CZ-10%, CZ-15% nanocomposites.

### Characterization

X-ray diffraction (XRD) data were tested using a Bruker D8 Advanced X-ray powder diffractometer (Rigaku Corp, Tokyo, Japan) with Cu-K $\alpha$  radiation ( $\lambda = 1.5418 \text{ \AA}$ ). The morphologies of the as-prepared samples were analyzed using scanning electron microscopy (SEM, S-4800, Hitachi, Tokyo, Japan). The crystal structures were observed using a JEM-2100 F transmission electron microscopy (TEM, JEOL, Japan). X-ray photoelectron spectroscopy (XPS) analyses were obtained on X-ray Photoelectron Spectrometer (ESCALAB250XI). Room temperature photoluminescence (PL) spectra were collected at the spectrophotometer (F97Pro, Lenggung, Shanghai) apparatus with excitation wavelength of 325nm.

### Photocatalytic hydrogen production activity

In this process, we first weighed 50mg catalyst dispersed in a mixed solution containing 0.35M  $\text{Na}_2\text{S}$  and 0.25M  $\text{Na}_2\text{SO}_3$ , continuously stirred for dispersion, and then sealed the device. Purge the solution with  $\text{N}_2$  for 30min. Under the ultraviolet light source provided by a 300W Xe lamp (PLS-SXE300 UV, Beijing Perfect light Co., Ltd., Beijing, China), hydrogen was generated via irradiation. The entire reaction was kept at 15 °C. Gas chromatography with  $\text{N}_2$  as carrier gas was used for detection every 2 hours.

## Result and Discussion

The phase of the composite nanomaterials was determined by XRD. ZnS, CuS / ZnS, ZC-5 %, ZC-10%. ZC-15% nanocomposites exhibit strong diffraction peaks at 27.12°, 28.55°, 30.62°, 47.75° and 56.69° Figure 1 corresponding to (100), (002), (101), (110) and (112) plane fit well with wurtzite-2H ZnS (JCPDS#36-1450), respectively. The peak intensity of pure ZnS is strong, indicating that the crystallinity of ZnS is good, and the other peaks are relatively weak. The peak intensity of CuS / ZnS is weaker than that of pure ZnS, which indicates that the cation exchange between  $\text{Cu}^{2+}$  and  $\text{Zn}^{2+}$  changes the peak intensity. The CuS particles are dispersed on ZnS, which has a certain masking effect on ZnS, resulting in less exposed crystals. However, no characteristic peak of CuS was observed. This may be due to the low concentration of CuS nanoparticles when compared to the ZnS that was uniformly distributed over the ZnS [34]. The XRD patterns of ZnS, CuS/ZnS, ZC-5%, ZC-10%, ZC-15% and pure ZnS are basically the same, and no characteristic peak of  $g\text{-C}_3\text{N}_4$  is shown which may be due to the lower loading of  $g\text{-C}_3\text{N}_4$  in the metal sulfide composites [35]. When the loading of  $g\text{-C}_3\text{N}_4$

reaches 15wt%, the characteristic peaks of ZnS and  $g\text{-C}_3\text{N}_4$  are basically the same and overlap with each other, resulting in the disappearance of  $g\text{-C}_3\text{N}_4$  characteristic peaks.

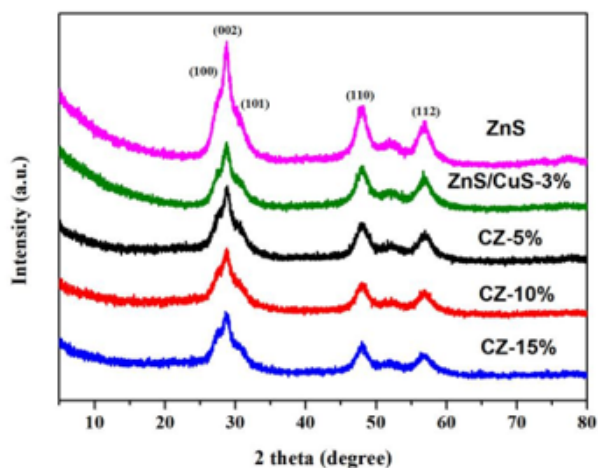


**Figure 1:** XRD patterns of ZnS, ZnS/CuS-3%, CZ-5%, CZ-10%, CZ-15%.

Chemical composition and the chemical oxidation states of the CZ-5% composite were obtained from the XPS Spectra. Figure 2(a-e) shows the high resolution XPS spectra of the elements Zn 2p, S 2p, C 1s and N 1s Cu 2p. The high-resolution Zn 2p Figure 2a of CZ-5 composite nanomaterials has two peaks at the binding energy values of 1022.35 eV and 1045.38 eV, which is caused by the splitting of Zn  $2p_{3/2}$  and Zn  $2p_{1/2}$ , indicating that it is  $\text{Zn}^{2+}$ . Similarly, the Cu 2p Figure 2e has two splitting peaks at the binding energy values of 933.10 eV and 952.99 eV due to Cu  $2p_{3/2}$  and Cu  $2p_{1/2}$ . It is consistent with the binding energy of  $\text{Cu}^{2+}$ . CuS was formed by cation exchange

between  $\text{Zn}^{2+}$  and  $\text{Cu}^{2+}$ . The binding energies of S 2P Figure 2b are 161.8 eV and 162.89 eV, but the displays the peaks at 163.85 eV and 162.58 eV accountable to  $\text{S}^{2-}2p_{1/2}$  and  $\text{S}^{2-}2p_{3/2}$  as per the report of CuS / ZnS catalyzed [36], This is due to the red shift of the binding energy caused by the defect ZnS prepared above. In high resolution XPS spectrum of C 1s Figure 3(a-d), two deconvolution peaks at 284.88 and 288.51 eV are observed, which are assigned to graphite C-C bonds and  $\text{sp}^2$ -hybridized carbon in N-containing aromatic ring (N-C=N) [37], respectively. Figure 4(a,b) shows the high-resolution N 1s spectrum comprising of three separate binding energies. The observed peaks at 399.67, 398.30 and 397.82 eV confirms the presence of C-NH, N-(C)<sub>3</sub> and C-N-C groups, respectively [37]. The morphology of defective ZnS, ZnS/CuS and CuS/ZnS/ $g\text{-C}_3\text{N}_4$  was analyzed by SEM. Figure 3a shows that the defect ZnS is flower cluster and spherical structure by scanning electron microscopy. It is confirmed by Figure 3b that CuS/ZnS keeps the shape of the flower cluster basically unchanged, and CuS clusters are embedded on its surface. After loading  $g\text{-C}_3\text{N}_4$ , the flake  $g\text{-C}_3\text{N}_4$  was loaded on the defective spherical ZnS, and the CuS/ZnS/ $g\text{-C}_3\text{N}_4$  Figure 3c ternary loaded nanocomposites with defective ZnS as the carrier were prepared. In order to further analyze the composition of the material, we adopted TEM to further explain the interaction between ZnS, CuS and  $g\text{-C}_3\text{N}_4$  in CuS/ZnS/ $g\text{-C}_3\text{N}_4$  (ZC-5%). We analyze the crystal atomic spacing, as shown in Figure 3d. The atomic spacing of 0.315nm observed in the (002) growth direction is mainly due to the hexagonal phase of zinc sulfide. It can also be found that the atomic spacing of 0.298nm corresponds to the cubic copper sulfide grown in the (103) direction. The maximum atomic spacing is 0.336nm, corresponding to  $g\text{-C}_3\text{N}_4$ , which proves that the CuS/ZnS/ $g\text{-C}_3\text{N}_4$  ternary composite material is well formed.

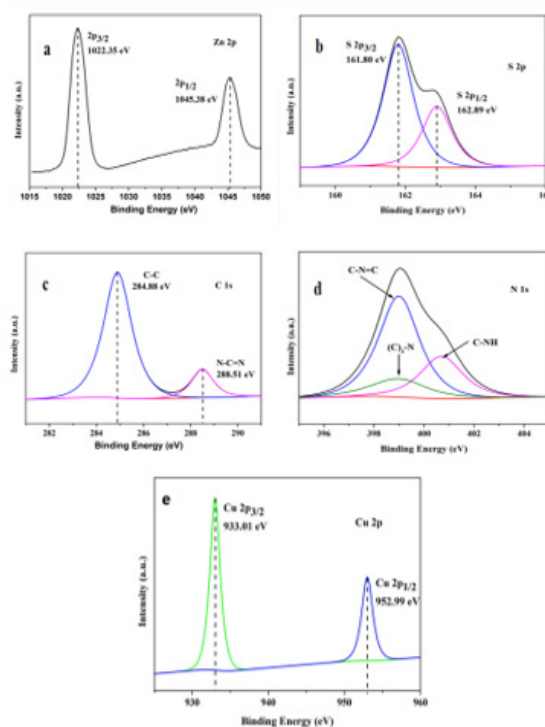


**Figure 2:** The corresponding high-resolution XPS spectra of (a) Zn 2p(b) S 2p(c) C 1s(d) N 1s and (e) Cu 2p.

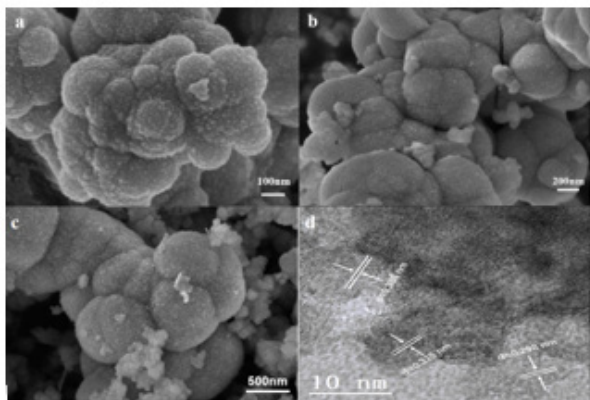


**Figure 3:** SEM images of ZnS(a), ZnS/CuS(b), CZ-5%(c) and TEM images of CZ-5%(d).

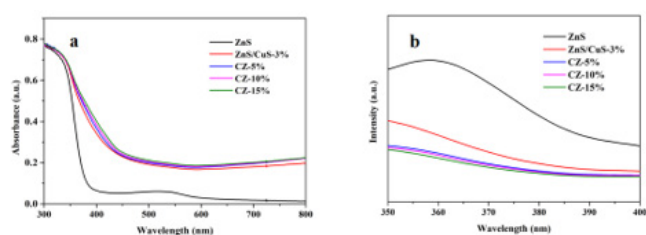


**Figure 4:** UV-vis absorption (a) and PL spectra (b) of ZnS, ZnS/CuS-3%, CZ-5%, CZ-10%, CZ-15%.

The synthesized photocatalyst was analyzed by UV-Vis. Figure 4a shows the absorption spectra of defective ZnS, ZnS/CuS-3%, CZ-5%, CZ-10%, and CZ-15%. It can be seen from the graph that after loading CuS, the absorption of visible light is significantly enhanced, which is mainly due to the formation of a heterojunction between a small amount of CuS and ZnS, which enhances the absorption characteristics of visible light. After loading  $g\text{-C}_3\text{N}_4$ , the visible light performance of the composite material is slightly improved compared with CuS/ZnS and increases with the increase of loading  $g\text{-C}_3\text{N}_4$ . As shown in Figure 4b, by testing the fluorescence of defective ZnS, ZnS / CuS-3%, CZ-5%, CZ-10% and CZ-15%, the intensity of ZnS fluorescence is generated by the transfer of photogenerated electrons on the valence band back to the conduction band and the hole is recombined, or through the non-radiative energy level transition to the corresponding sulfur vacancy, and finally transferred back to the valence band to achieve the re-combination of carriers. The higher the intensity, the stronger the binding ability of photogenerated electrons and holes, which is not conducive to photocatalytic reaction. When the material is loaded with CuS, the binding strength between the photogenerated electrons and holes is significantly reduced, which is due to the formation of heterojunctions, which enables the effective separation of electrons and holes. After loading  $g\text{-C}_3\text{N}_4$ , its strength is significantly reduced, which indicates that the ternary composite has better electron and hole separation ability.

In order to further study the band gap of different nanocomposites, we obtained Kubelka-Munk formula conversion, as shown in Figure 5.

$$A = -\lg(R) \quad (\text{formula 1})$$

$$F(R) = (1-R)^2 / 2R \quad (\text{formula 2})$$

where A in Formula 1 represents the absorbance of the sample, and R is the theoretical reflection value of Kubelka-Munk.

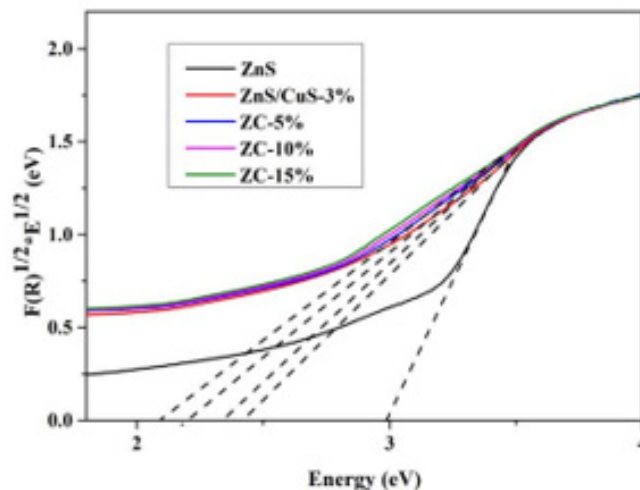


**Figure 5:** Kubelka-Munk diagrams of different nanocomposite semiconductors..

The band gaps of ZnS, ZnS/CuS-3%, CZ-5%, CZ-10%, CZ-15% can be obtained by doing their tangents. In the figure, we use  $E$  ( $1240/\lambda$ ) as the abscissa and  $F(R)^{1/2} \cdot E^{1/2}$  as the ordinate. The band gaps of ZnS, ZnS/CuS-3%, CZ-5%, CZ-10% and CZ-15% are 2.99, 2.43, 2.34, 2.21, 2.09 eV, respectively. Among them, CZ-15% has the smallest band gap, and ZnS without any modification has the largest band gap. This shows that the construction of ternary heterojunction can effectively reduce the band gap of photocatalyst and can effectively utilize solar energy.

In order to better understand the photocatalytic hydrogen production effect of ZnS, ZnS-CuS-3%, CZ-5%, CZ-10%, CZ-15% nanocomposites, we used an aqueous solution of 0.25M sodium sulfide and 0.35M sodium sulfite as a sacrificial agent to assist hydrogen production. This experiment was only carried out under visible light, in order to better fit the use of solar energy. As shown in Figure 6, for ZnS, ZnS / CuS-3%, CZ-5%, CZ-10%, CZ-15% nanocomposites, their hydrogen production were detected to be 0, 1784.21, 2265.87, 2030.80, 2128.24  $\mu\text{mol/g.h}$ , respectively. ZnS as a photocatalyst did not detect the production of  $\text{H}_2$  in the process of hydrogen production. The main reason is that the energy gap of ZnS is too large, and the energy provided by light cannot excite ZnS to produce electrons, so that  $\text{H}^+$  cannot be reduced to produce  $\text{H}_2$ . Compared with ZnS, the hydrogen production of ZnS/CuS-3% achieved a breakthrough of 0 under visible light, mainly due to the formation of heterojunction between ZnS and CuS. The light absorption ability of ZnS/CuS-3% was greatly improved by the visible light absorption of solid ultraviolet spectrum, which not only reduced the band width, but also effectively promoted the separation of electrons and holes. In order to more intuitively reflect the influence of  $g\text{-C}_3\text{N}_4$  on ZnS/CuS heterojunction, we loaded  $g\text{-C}_3\text{N}_4$  in CuS/ZnS/ $g\text{-C}_3\text{N}_4$  with 5, 10, 15wt%, respectively.

Under different loadings, the photocatalytic hydrogen production performance of CZ-5% nanocomposites is the best, and its hydrogen production efficiency is 2265.87  $\mu\text{mol/g}\cdot\text{h}$ . However, with the increase of  $g\text{-C}_3\text{N}_4$  content, the hydrogen production of CZ-10%, CZ-15% nanocomposites gradually decreases, which is mainly due to the excessive  $g\text{-C}_3\text{N}_4$  covering ZnS/CuS, affecting its hydrogen production performance. However, in general, the hydrogen production of CZ-10% and CZ-15% nanocomposites is still higher than that of photocatalyst ZnS/CuS-3%. It is proved that the construction of ternary heterojunction can not only improve the utilization of light, but also promote the photocatalytic water splitting to produce hydrogen.

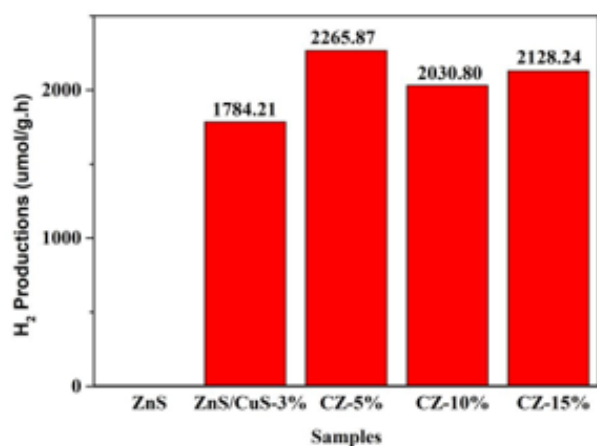


**Figure 6:** Photocatalytic hydrogen production rate of ZnS, ZnS/CuS-3%, CZ-5%, CZ-10%, CZ-15%.

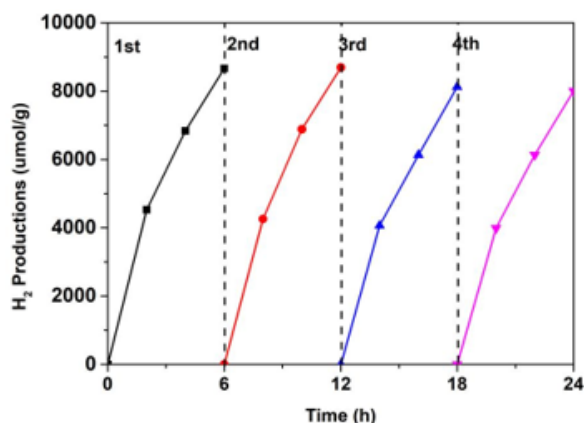


**Figure 7:** Reusability of CZ-5CN photocatalysts for four run cycles.

In order to further test the stability of the synthesized nanocomposites for sustainable hydrogen production, we carried out a continuous photocatalytic reaction on the best performance CZ-5%, which was cycled once every 6 hours for a total of four cycles. We used an aqueous solution of 0.25M sodium sulfide and 0.35M sodium sulfite as a sacrificial agent for hydrogen production assistance. This experiment was only performed under visible light. The same photocatalyst was used for hydrogen production test. Each time, the catalyst was only filtered and dried, and the obtained catalyst was basically not lost, and then the reaction was repeated. It can be clearly seen from the Figure 7 that the hydrogen production of

the first two reactions is basically the same, and the third and fourth times decrease slightly, but its photocatalytic hydrogen production performance is still efficient, indicating that the obtained catalyst has good stability and has certain application value. Subsequently, we re-recycled the nanocomposite photocatalyst and carried out XRD test. The diffraction peak intensity was basically consistent with that before the reaction, indicating that the nanocomposite photocatalyst can be used for continuous photocatalytic hydrogen production reaction.

In order to further explore the effect of different types of heterojunctions on the separation ability of electrons and holes, samples ZnS/CuS and ZC-5% were selected for transient photocurrent response test. As shown in Figure 8(a,b), when the light source irradiates the semiconductor nanomaterials, the samples have good light responsiveness, and the photogenerated carriers are quickly excited. However, the photocurrent response of the semiconductor catalyst ZC-5% is slightly higher than that of ZnS/CuS, indicating that the loading of  $g\text{-C}_3\text{N}_4$  has little ability to hinder the recombination of electrons and holes. Next, we further explore the process of interfacial charge transport. We tested the electrochemical impedance of ZnS, ZnS/CuS-3%, CZ-5%, CZ-10%, CZ-15%. In the figure, we can clearly observe that the radius of ZC-10% nanocomposites is smaller than that of other photocatalytic materials, indicating that the resistance of surface charge transfer is the smallest, which is conducive to the rapid transfer of photogenerated carriers. In summary, the two groups of electrochemical tests show that the construction of heterojunction by loading  $g\text{-C}_3\text{N}_4$  has a certain improvement in promoting the use of visible light.

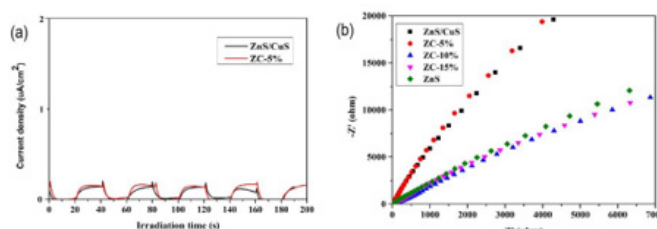


**Figure 8:** Instantaneous photocurrent response(a) and electrochemical impedance(b).

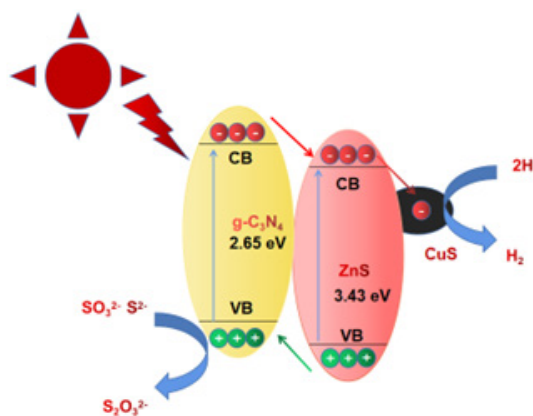


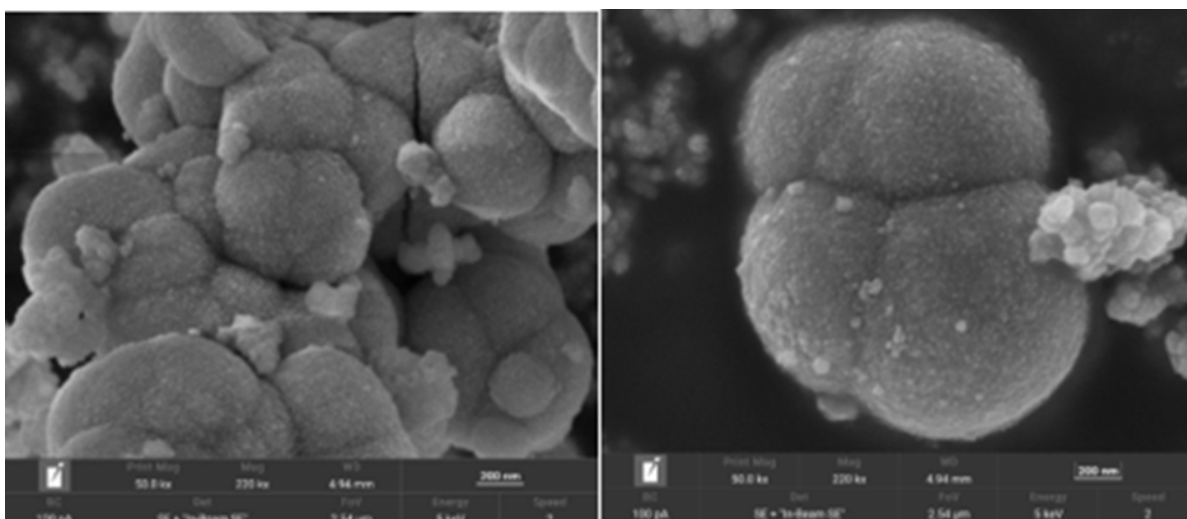
**Figure 9:** Plausible mechanism for hydrogen production over CuS/ZnS/ $g\text{-C}_3\text{N}_4$  photocatalyst.

Through the above test results and analysis, we explored the rational mechanism of photocatalytic hydrogen production of CuS/ZnS/g-C<sub>3</sub>N<sub>4</sub> nanocomposites, as shown Figure 9. Initially, due to the wide band gap of ZnS, it cannot respond well to visible light, and can only perform photocatalytic hydrogen production under ultraviolet light irradiation, which cannot meet our efficient use of sunlight. Therefore, we loaded CuS on the surface of ZnS by cation exchange method to form a heterojunction of zinc sulfide and copper sulfide. The loading of copper sulfide not only makes the catalyst have good responsiveness to visible light, but also effectively improves the efficiency of photogenerated electrons and reduces the recombination rate of electrons and holes. In order to further expand the range of visible light absorption, zinc sulfide and copper sulfide nano-catalysts were dispersed on g-C<sub>3</sub>N<sub>4</sub> with a band gap of only 2.65 eV by ultrasonic dispersion method. When the light source is irradiated on the catalyst, since the potential of the g-C<sub>3</sub>N<sub>4</sub> conduction band is negative to the potential of ZnS/CuS, the electrons on the conduction band generated from the photoexcitation of g-C<sub>3</sub>N<sub>4</sub> will be transferred to ZnS/CuS with lower potential, which greatly reduces the recombination of electrons and

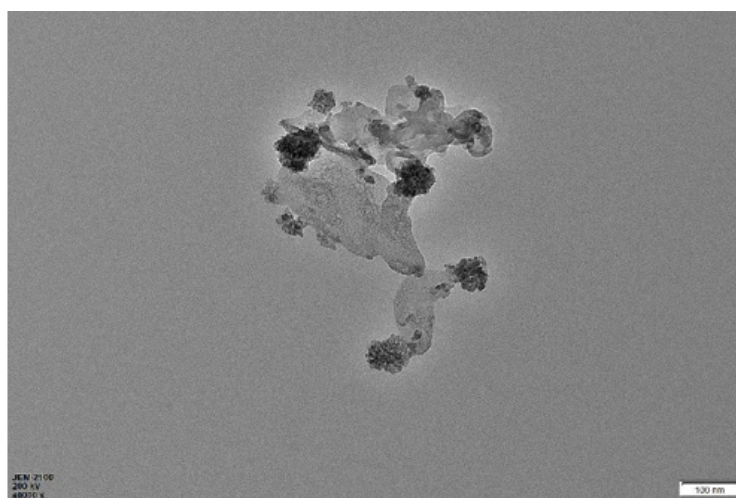
holes on g-C<sub>3</sub>N<sub>4</sub>. Moreover, the conduction band position of ZnS/CuS is more negative than that of H<sup>+</sup>/H<sub>2</sub> (0 eV vs NHE), which meets the potential requirements for hydrogen generation. The electrons on the conduction band of ZnS/CuS combine with the free H<sup>+</sup> in water to generate H<sub>2</sub>, and the holes generated on ZnS are transferred to the valence band of g-C<sub>3</sub>N<sub>4</sub> with lower potential, which is utilized by the sacrificial agent.

## Conclusion

The experimental results show that a novel CuS/ZnS/g-C<sub>3</sub>N<sub>4</sub> ternary composite material synthesized by hydrothermal method, cation exchange method and ultrasonic assisted synthesis is a very efficient photocatalyst. Among them, g-C<sub>3</sub>N<sub>4</sub> containing 5 wt% has a hydrogen production effect of 2265.87 μmol/g.h under visible light, which has a good photocatalytic hydrogen production effect, mainly due to the formation of CuS/ZnS/g-C<sub>3</sub>N<sub>4</sub> ternary heterojunction, which effectively inhibits the recombination of electrons and holes. This is the first ternary heterojunction composite for defective zinc sulfide.



This is part of the SEM image of the material.



This is a partial TEM image of the material.

## References

- Fujishima A, Honda K (1972) Electrochemical photolysis of water at a semiconductor electrode. *Nature* 238(5358): 37-38.
- Thammanoon S, Chompoonuch J, Sumaeth C (2009) Photocatalytic H<sub>2</sub> production from water splitting under visible light irradiation using eosin y-sensitized mesoporous-assembled Pt/TiO<sub>2</sub> nanocrystal photocatalyst. *Journal of Power Sources* 190(2): 513-524.
- Gao R, Jiao Z, Wang Y, Xu L, Xia S, et al. (2016) Eco-friendly synthesis of rutile TiO<sub>2</sub> nanostructures with controlled morphology for efficient lithium-ion batteries. *Chemical Engineering Journal* 304: 156-164.
- Li Y, Yi H, Tang X, Liu X, Wang Y, et al. (2016) Study on the performance of simultaneous desulfurization and denitrification of Fe<sub>3</sub>O<sub>4</sub>-TiO<sub>2</sub> composites. *Chemical Engineering Journal* 304: 89-97.
- Wang XJ, Yang WY, Li FT, Zhao J, Liu RH, et al. (2015) Construction of amorphous TiO<sub>2</sub>/BiOBr heterojunctions via facets coupling for enhanced photocatalytic activity. *Journal of Hazardous Materials* 292: 126-136.
- Arai T, Senda SI, Sato Y, Takahashi H, Shinoda K, et al. (2008) Cu-doped ZnS hollow particle with high activity for hydrogen generation from alkaline sulfide solution under visible light. *Chemistry of Materials* 20(5): 1997.
- Wang Y, Wu J, Zheng J, Rong X (2011) Highly active Zn<sub>x</sub>Cd<sub>1-x</sub>S photocatalysts containing earth abundant elements only for H<sub>2</sub> production from water under visible light. *Catal Sci Technol* 1(6): 940-947.
- Wang DH, Wang L, Xu AW (2012) Room-temperature synthesis of Zn<sub>0.80</sub>Cd<sub>0.20</sub>S solid solution with a high visible-light photocatalytic activity for hydrogen evolution. *Nanoscale* 4(6): 2046-2053.
- Wang Y, Wu J, Zheng J, Jiang R, Rong X (2012) Ni<sup>2+</sup>-doped Zn<sub>x</sub>Cd<sub>1-x</sub>S photocatalysts from single-source precursors for efficient solar hydrogen production under visible light irradiation. *Catalysis Science & Technology* 2(3): 581-588.
- Muruganandham M, Kusumoto Y (2009) Synthesis of N, C codoped hierarchical porous microsphere ZnS as a visible light-responsive photocatalyst. *J Phys Chem C* 113(36): 16144.
- Zhou Y, Chen G, Yu Y, Feng Y, Zheng Y, et al. (2015) An efficient method to enhance the stability of sulphide semiconductor photocatalysts: A case study of N-doped ZnS. *Physical Chemistry Chemical Physics* 17(3): 1870-1876.
- Zhang J, Wang Y, Jun Z, Lin Z, Feng H, et al. (2013) Enhanced photocatalytic hydrogen production activities of Au-loaded ZnS flowers. *ACS Appl Mater Inter* 5(3): 1031-1037.
- Shen Z, Chen G, Wang Q, Yu Y, Zhou C, et al. (2012) Sonochemistry synthesis and enhanced photocatalytic H<sub>2</sub>-production activity of nanocrystals embedded in CdS/ZnS/In<sub>2</sub>S<sub>3</sub> microspheres. *Nanoscale* 4(6): 2010-2017.
- Zhang S, Cai Y, He H, Zhang Y, Liu R, et al. (2016) Heteroatom doped graphdiyne as efficient metal-free electrocatalyst for oxygen reduction reaction in alkaline medium. *Journal of Materials Chemistry A Materials for energy and sustainability* 4(13): 4738-4744.
- Jang ES, Won JH, Hwang SJ, Choy JH (2006) Fine tuning of the face orientation of ZnO crystals to optimize their photocatalytic activity. *Advanced Materials* 18(24): 3309-3312.
- Mclaren A, Valdes ST, Li G, Tsang SC (2009) Shape and size effects of ZnO nanocrystals on photocatalytic activity. *Journal of the American Chemical Society* 131(35): 12540-12541.
- Goswami DY, Stefanakos E, Batzill M, Kislov N, Lahiri J, et al. (2009) Photocatalytic degradation of methyl orange over single crystalline ZnO: Orientation dependence of photoactivity and photostability of ZnO. *Langmuir* 25(5): 3310-3315.
- Xu T, Hong Z, Zhang P, Wei L (2016) Photocatalytic degradation of a low concentration pharmaceutical pollutant by nanoporous TiO<sub>2</sub> film with exposed {001} facets. *RSC Advances* 6(98): 95818-95824.
- Yao X, Hu X, Liu Y, Wang X, Wang D, et al. (2020) Simultaneous photocatalytic degradation of ibuprofen and H<sub>2</sub> evolution over Au/sheaf-like TiO<sub>2</sub> mesocrystals. *Chemosphere* 261: 127759.
- Ming K, Li Y, Chen X, Tian T, Zhao X, et al. (2011) Tuning the relative concentration ratio of bulk defects to surface defects in TiO<sub>2</sub> nanocrystals leads to high photocatalytic efficiency. *Journal of the American Chemical Society* 133(41): 16414-16417.
- Liu G, Yang HG, Wang X, Cheng L, Lu H, (2009) Enhanced photoactivity of oxygen-deficient anatase TiO<sub>2</sub> sheets with dominant {001} facets. *The Journal of Physical Chemistry C*.
- Junpeng W, Zeyan W, Baibiao H, Yandong M, Yuanyuan L, et al. (2012) Oxygen vacancy induced bandgap narrowing and enhanced visible light photocatalytic activity of ZnO. *ACS Applied Materials & Interfaces* 4(8): 4024-4030.
- Lv Y, Yao W, Ma X, Pan C, Zong R, et al. (2013) The surface oxygen vacancy induced visible activity and enhanced UV activity of a ZnO<sub>1-x</sub> photocatalyst. *Catalysis science & technology* 12(3): 3136-3146.
- Wang P, Wang D, Lin J, Li X, Peng C, et al. (2012) Lattice defect-enhanced hydrogen production in nanostructured hematite-based photoelectrochemical device. *ACS Applied Materials & Interfaces* 4(4): 2295-2302.
- Lv M, Sun X, Wei S, Shen C, Mi Y, et al. (2017) Ultrathin lanthanum tantalate perovskite nanosheets modified by nitrogen doping for efficient photocatalytic water splitting. *ACS Nano* 11(11): 11441-11448.
- Shaowen C, Jianguo Y (2014) g-C<sub>3</sub>N<sub>4</sub>-Based Photocatalysts for Hydrogen Generation. *Journal of Physical Chemistry Letters*.
- Wen MQ, Xiong T, Zang ZG, Wei W, Tang XS, et al. (2016) Synthesis of MoS<sub>2</sub>/g-C<sub>3</sub>N<sub>4</sub> nanocomposites with enhanced visible-light photocatalytic activity for the removal of nitric oxide (NO). *Optics Express* 24(10): 10205-10212.
- Zhang Z, Liu K, Feng Z, Bao Y, Dong B (2016) Hierarchical sheet-on-sheet ZnIn<sub>2</sub>S<sub>4</sub>/g-C<sub>3</sub>N<sub>4</sub> heterostructure with highly efficient photocatalytic H<sub>2</sub> production based on photoinduced interfacial charge transfer. *Sci Rep* 6: 19221.
- Wei X, Shao C, Li X, Na L, Wang K, et al. (2016) Facile in situ synthesis of plasmonic nanoparticles-decorated g-C<sub>3</sub>N<sub>4</sub>/TiO<sub>2</sub> heterojunction nanofibers and comparison study of their photosynergistic effects for efficient photocatalytic H<sub>2</sub> evolution. *Nanoscale* 8(21): 11034-11043.
- Wang Y, Zhang J, Wang X, Antonietti M, Li H (2010) Boron- and fluorine-containing mesoporous carbon nitride polymers: Metal-free catalysts for cyclohexane oxidation. *Angewandte Chemie International Edition* 49(19): 3356-3359.
- Liu G, Niu P, Sun C, Smith SC, Chen Z, et al. (2010) Unique electronic structure induced high photoreactivity of sulfur doped graphitic C<sub>3</sub>N<sub>4</sub>. *Journal of the American Chemical Society* 132(33): 11642-11648.
- Zhang Z, Huang J, Fang Y, Zhang M, Liu K, et al. (2017) Nonmetal Plasmonic Z-Scheme Photocatalyst with UV- to NIR-Driven Photocatalytic Protons Reduction. *Advanced Materials* 29(18): 1606688.
- Hong Y, Zhang J, Huang F, Zhang J, Wang X, et al. (2015) Enhanced visible light photocatalytic hydrogen production activity of CuS/ZnS nanoflower spheres. *Journal of Materials Chemistry A* 3(26): 13913-13919.
- Lei G, Changcun H, Jing L (2011) Novel visible light-induced g-C<sub>3</sub>N<sub>4</sub>/Bi<sub>2</sub>WO<sub>6</sub> composite photocatalysts for efficient degradation of methyl orange. *Applied Catalysis B Environmental* 108-109: 100-107.
- Mai TT, Schultze JW, Staikov G, Munoz AG (2005) Mechanism of galvanic metallization of CoS-activated insulating polymer surfaces. *Thin Solid Films* 488(1-2): 321-328.
- Qin ZQ, Zhang FJ (2013) Surface decorated Cd<sub>1-x</sub>Zn<sub>x</sub>S cluster with CdS quantum dot as sensitizer for highly photocatalytic efficiency. *Applied Surface Science* 285(Part-B): 912-917.
- Ye L, Liu J, Jiang Z, Peng T, Zan L (2013) Facets coupling of BiOBr-g-C<sub>3</sub>N<sub>4</sub> composite photocatalyst for enhanced visible-light-driven photocatalytic activity. *Applied Catalysis B Environmental* 142-143: 1-7.